

# 1 **Airborne laser scanning transects over Canada's northern** 2 **forests: lidar plots for science and application**

3 Christopher W. Bater<sup>1</sup>, Joanne C. White<sup>1</sup>, Hao Chen<sup>1</sup>, Piotr Tompalski<sup>1</sup>, Txomin Hermosilla<sup>1</sup>,  
4 Michael A. Wulder<sup>1</sup>

5 <sup>1</sup>Canadian Forest Service (Pacific Forestry Centre), Natural Resources Canada, 506 West Burnside Road, Victoria,  
6 British Columbia, Canada

7 *Correspondence to:* Christopher W. Bater (christopher.bater@nrcan-rncan.gc.ca)

8 **Abstract** Mapping vegetation is required for monitoring the condition of forest resources. Satellite data provide  
9 information on land cover and change; however, forest structural attributes are difficult to model without additional  
10 measurements from ground plots or airborne laser scanning (ALS, also known as airborne light detection and  
11 ranging or lidar) instruments. Over large and inaccessible areas, such as Canada's northern and predominantly  
12 unmanaged forests, ground plots are expensive, difficult to install, and unlikely to form a statistically valid  
13 probability sample. An alternative means to obtain information regarding forest structure in these situations is  
14 samples of ALS (hereafter lidar plots). Transect-based samples of ALS data can be used to provide structural  
15 information for the calibration and validation of spatially explicit predictive modelling for wide-area mapping of  
16 forest attributes. Here we describe and share data from the recent acquisition and processing of ALS transects across  
17 Canada's northern forests. Approximately 55,000 km of ALS transects have been acquired in 2023, 2024, and 2025.  
18 Acquisition specifications included minimum swath widths of 500 m (year 2023) or 800 m (2024 and 2025), with a  
19 minimum pulse density of 12 pulses/m<sup>2</sup>. Acquisition flight lines were designed to sample a range of northern forest  
20 conditions and to correspond with a concurrent ground plot sampling campaign. Airborne laser scanning data were  
21 processed into height-normalized point clouds and reprojected to a custom Lambert conformal conic projection to  
22 align with existing national satellite information products. More than 15 million 900 m<sup>2</sup> lidar plots were generated  
23 from the 2023 transect dataset with point cloud metrics (i.e., area-based statistical summaries of the ALS point  
24 cloud) calculated for each 30 by 30 m cell. Presently, the 2023 lidar plots and their associated point cloud metrics  
25 are stored in openly available SQLite GeoPackages, with additional annual transect collections to be added as  
26 available. To accommodate a wide range of users and applications, both comprehensive and abridged versions of the  
27 metric databases, with 369 metrics and 40 metrics, respectively, are shared. The framework underlying this dataset  
28 is fully transferable to other regions with comparable information needs. The flexible data structure used allows  
29 seamless integration of additional open-access ALS transect data as new acquisitions and processing become  
30 available. By providing detailed, scalable measurements that bridge the gap between ground observations and wall-  
31 to-wall satellite information products, this open-access resource empowers both the scientific and operational  
32 forestry communities. These data will drive the development of enhanced wildfire fuels maps, comprehensive forest

33 inventories, and robust carbon products, supporting informed decision making and advancing sustainable forest  
34 management.

## 35 **1 Introduction**

36 Vegetation structure underpins a range of ecological, social, and economic forest values, including timber  
37 harvesting, carbon sequestration, biodiversity, water quality, and wildfire fuels (Haslem et al., 2011; Keith et al.,  
38 2009; Tews et al., 2004). Medium resolution satellite remote sensing (i.e., pixels sided 10 – 100 m) has proven  
39 effective for the wall-to-wall mapping of land cover (Hermosilla et al., 2022; Vogelmann et al., 2001), monitoring  
40 disturbance and recovery (Hansen et al., 2014; White et al., 2017b), and more recently modelling attributes such as  
41 species (Hermosilla et al., 2024). The characterization of vegetation structure, however, can be modeled using pixel-  
42 based, optical remotely sensed data (Coops et al., 2021), but not with the accuracies possible using light detection  
43 and ranging (lidar) technologies, particularly airborne laser scanning (ALS). It is not entirely fair to compare optical  
44 satellite remote sensing and ALS due to their differences in data costs to the end user, the level of detail captured,  
45 and the intensity and repeatability of collection (Fassnacht et al., 2024). However, ALS provides access to  
46 simultaneous measurements of the vertical distribution of vegetation and the underlying terrain morphology (Lefsky  
47 et al., 2002), providing critical information on forest complexity and condition that cannot be obtained through other  
48 remote sensing methods.

49 Investigations related to ALS and forest measurement have been ongoing since the 1980s (Aldred and Bonnor, 1985;  
50 Nelson, 2013), and by the early 2000s the technology was recognized as a robust tool for estimating inventory  
51 attributes related to vegetation structure (Næsset, 2004; Reutebuch et al., 2005; Wulder et al., 2008). Given the high  
52 cost and limited access to airborne lidar instruments in the early years, many initial investigations adopted  
53 probability sampling approaches to efficiently obtain representative data (Wulder et al., 2012b). In contrast, today  
54 many Canadian jurisdictions are actively collecting wall-to-wall ALS data to support the development of enhanced  
55 forest inventories; however, data acquisitions are typically focused on managed forests in the south, leaving remote,  
56 northern forests underrepresented (White et al., 2025). Stinson et al. (2019) define forest management status in  
57 Canada using ownership, protection status, and tenure as these three characteristics are "...related to forest  
58 management interests, governance and objectives in a generalized way across all Canadian jurisdictions" (p. 103).  
59 Definitions of managed forest are different for carbon accounting purposes wherein unmanaged forests are excluded  
60 from reporting requirements (Ogle et al., 2018). Although they are not actively managed, northern forests are critical  
61 to the aforementioned forest values. The federal government reports on all forests, both managed and unmanaged, as  
62 implemented through the National Forest Inventory program and communicated via the annual State of the Forests  
63 report (Natural Resources Canada, 2023). As Canada's mean annual temperature has increased at more than twice  
64 the global rate (Bourdeau-Goulet and Hassanzadeh, 2021), northern forests are particularly vulnerable to increased  
65 wildfire risk (Burton, 2023; Parisien et al., 2023), further underscoring the need to improve available information for  
66 these forests.

67 Although typically flown in a wall-to-wall configuration, ALS data may be collected as sampled linear transects to  
68 extend structural information over remote areas where continuous, wall-to-wall coverage is impractical. Wulder et  
69 al. (2012b) described lidar sampling as a cost-effective alternative to wall-to-wall lidar acquisition for large-area  
70 forest monitoring. The authors demonstrated that statistically sound sampling and inference methods can enable  
71 robust characterizations of forest structure, and that integration of lidar samples with field and satellite data can  
72 enhance scalability and precision of estimates. For example, Andersen et al. (2011) presented a methodology for  
73 estimating forest biomass over a large area of interior Alaska. The authors used a combination of ground plots and  
74 sampled ALS transects to achieve reasonable precision, underscoring the cost-efficiency of integrating partial  
75 airborne lidar coverage. Also working in Alaska, Babcock et al. (2018) demonstrated that sparse lidar transects,  
76 when fused with field plots and Landsat tree cover in a Bayesian geostatistical framework, can yield wall-to-wall  
77 biomass maps with quantified uncertainty. Nelson et al. (2012) used an airborne profiling lidar to estimate forest  
78 biomass in Norway and found that the results were similar to those obtained through ground surveys. Building on  
79 this logic, Margolis et al. (2015) employed a three-phase sampling design combining ground plots, airborne  
80 profiling lidar, and ICESat-GLAS satellite lidar data to estimate biomass across the North American boreal forest.

81 Wulder et al. (2012a) proposed the concept of lidar plots, wherein lidar transect data, augmented by ground plot  
82 information, provide sample-based characterizations of forest structure. Lidar plot locations are established within  
83 sampled lidar transect swaths at a spatial resolution matching the typical size (area) of tall tree ground plots or the  
84 pixel size of medium spatial resolution remotely sensed data (e.g., pixels sized 400-900 m<sup>2</sup>). The ALS data are  
85 processed to generate a suite of summary statistics or metrics that characterize the point cloud within each lidar plot  
86 (e.g., mean height, maximum height, percentiles of height). Using an area-based approach (ABA) (Næsset, 2002;  
87 White et al., 2013), a sample of co-located ground plot measurements are then used with the point cloud metrics to  
88 generate predictions of inventory attributes of interest such as height, basal area, volume, or biomass, among others.  
89 These lidar plots, with associated metrics and attributes, may then be linked to other remotely sensed data (e.g.,  
90 optical time series) via imputation, enabling the generation of spatially exhaustive and spatially explicit models of  
91 forest structure ultimately resulting in maps representing large areas (Coops et al., 2021; Wulder et al., 2012a).

92 In a proof-of-concept study, Zald et al. (2016) demonstrated how lidar plots could be used as a surrogate for ground  
93 plots to map a suite of point cloud height (mean, standard deviation, coefficient of variation, 95<sup>th</sup> percentile) and  
94 cover metrics (percentage of first returns > 2 m, percentage of first returns > mean height), as well as select forest  
95 inventory attributes (Lorey's tree height, basal area, gross stem volume, and total aboveground biomass) for a ~38  
96 million ha forest region in Saskatchewan, Canada for the year 2010 (corresponding to the year of ALS acquisition).  
97 Zald et al. (2016) availed upon 1,560 km of lidar transects and a set of 4,340 lidar plots to impute point cloud  
98 metrics directly, with the ABA forest attributes carried as ancillary variables in the plot-matching process.

99 Expanding on this approach, Matasci et al. (2018a) employed >25,000 km of lidar transects and 80,687 lidar plots  
100 with Landsat surface reflectance composites to produce boreal-wide maps (~552 million ha) of the same point cloud  
101 metrics and forest structural attributes as Zald et al. (2016) for the year 2010. Matasci et al. (2018b) further extended  
102 this approach in both space and time, mapping forest structure annually for the entirety of Canada's forested

103 ecosystems (~650 million ha) for each year from 1984 to 2016. Matasci et al. (2018b) availed upon seven different  
104 lidar acquisitions and associated lidar plots (n = 84,482) to achieve national, annual maps of forest structure, thereby  
105 enabling characterization of structural dynamics in both disturbed and undisturbed forests over the three-decade  
106 period considered. Matasci et al. (2018b) also used a completely independent set of lidar plots, derived from  
107 separate lidar acquisitions to validate the imputed attributes, both spatially and temporally. Collectively, these  
108 studies demonstrate the utility of ALS sampling and lidar plots in generating spatially and temporally rich forest  
109 structural information at landscape to continental scales.

## 110 **1.1 Motivation**

111 Canada's boreal forests and the communities therein are increasingly exposed to wildfire risks (Parisien et al., 2020),  
112 yet many northern and remote regions lack detailed vegetation inventories essential for fire behavior modeling  
113 (Crowley et al., 2023; Parisien et al., 2020; Stinson et al., 2019). In these areas outside of the managed forest zone,  
114 accurate information on forest structure and fuel properties is limited, constraining the capacity to assess risk or plan  
115 mitigation strategies (Crowley et al., 2023). Further, the ongoing development of the next generation Canadian  
116 Forest Fire Danger Rating System (CFFDRS-2025) will incorporate new data sources and requires that a new suite  
117 of vegetation and soil attributes be modelled (Canadian Forest Service Fire Danger Group, 2021). Addressing this  
118 data gap requires spatially explicit maps of key forest structural attributes such as canopy bulk density and canopy  
119 base height which may be estimated using ALS (Andersen et al., 2005; Martin-Ducup et al., 2025; Moran et al.,  
120 2020; Riaño et al., 2004), but cannot be reliably derived from satellite imagery alone (Mutlu et al., 2008; Riaño et  
121 al., 2003) and which are equally difficult to estimate in the field (Keane et al., 2005).

122 To support this need, the Government of Canada via the Canadian Forest Service launched the Northern Forest  
123 Mapping program (NorthForM). Between 2023 and 2025, this initiative is acquiring ALS transects and coincident  
124 ground plot data (Boucher et al., 2023), with the goal of modeling fuel-related forest structure attributes for wall-to-  
125 wall mapping using satellite imagery (Coops et al., 2021). These methods build upon earlier work by the National  
126 Terrestrial Ecosystem Monitoring System (NTEMS), which was developed to monitor Canada's forested ecosystems  
127 on an annual basis using consistent, nationally available datasets (White et al., 2014; Wulder et al., 2024). The  
128 NTEMS relies primarily on medium spatial resolution satellite data (initially solely Landsat, now augmented with  
129 Sentinel 2) time series, integrated with ALS transects and ground plots, to generate national information products  
130 characterizing disturbance, land cover, and forest structure (Hermosilla et al., 2016). The first national lidar transect  
131 dataset was collected in 2010 to support NTEMS product development (Hopkinson et al., 2011; Wulder et al.,  
132 2012a), and subsequent work has shown that combining these data sources enables spatially comprehensive  
133 estimates of both forest structure and derived attributes (Matasci et al., 2018a, b; Zald et al., 2016)

## 134 **1.2 Objectives**

135 Herein, we describe the acquisition and processing of ALS transect data for Canada's northern forests, and the  
136 subsequent generation of 30 m lidar plots and ABA point cloud metrics. These data are being shared in an open

137 repository to support the development of models needed for generating wall-to-wall predictions of attributes relevant  
138 for characterizing forest structure and informing forest fuels mapping.

## 139 **2 Data and methods**

### 140 **2.1 Canada's northern forests**

141 Canada's unmanaged northern forests represent some of the largest natural treed ecosystems on Earth. Spanning  
142 northern Quebec, Ontario, Manitoba, Saskatchewan, Alberta, and significant portions of the Yukon and Northwest  
143 Territories, they are mostly free of large-scale industrial land uses such as forestry. Unlike managed forests to the  
144 south, these ecosystems are shaped primarily by natural disturbances such as wildfires and insect outbreaks,  
145 although the anthropogenic footprint is expanding in some areas (Wells et al., 2020). Tree species are cold-tolerant,  
146 primarily within the genera *Abies*, *Larix*, *Picea*, and *Pinus*, but also include *Populus* and *Betula*. Northern forests  
147 and treed areas are part of a larger mosaic which includes lakes, rivers, and wetlands, treeless alpine areas, maritime  
148 heathlands, and occasional grasslands (Brandt, 2009).

### 149 **2.2 Airborne laser scanning data acquisitions**

150 Planning for the 2023-2025 lidar acquisition considered previous experience with national ALS transects  
151 (Hopkinson et al., 2011), as well as recommendations from the Canadian airborne lidar acquisition guidelines (CSA  
152 Group, 2025). Acquisition specifications are summarized in Table 1. Due to the remoteness of the area of interest  
153 (Figure 1), the lack of permanent global navigation satellite system (GNSS) base station infrastructure, and the  
154 impracticality of setting up ad hoc base stations, precise point positioning (PPP) services were employed to correct  
155 ALS return coordinates. The target window for data acquisition was between 15 June and 15 September of each  
156 year, and linear mode lidar systems were required. The ALS data were collected by private sector vendors who were  
157 awarded contracts through the Government of Canada's competitive procurement process (Table 2). Each vendor  
158 used their own aircraft, sensors, and systems to collect data according to the specifications outlined in Table 1.

159

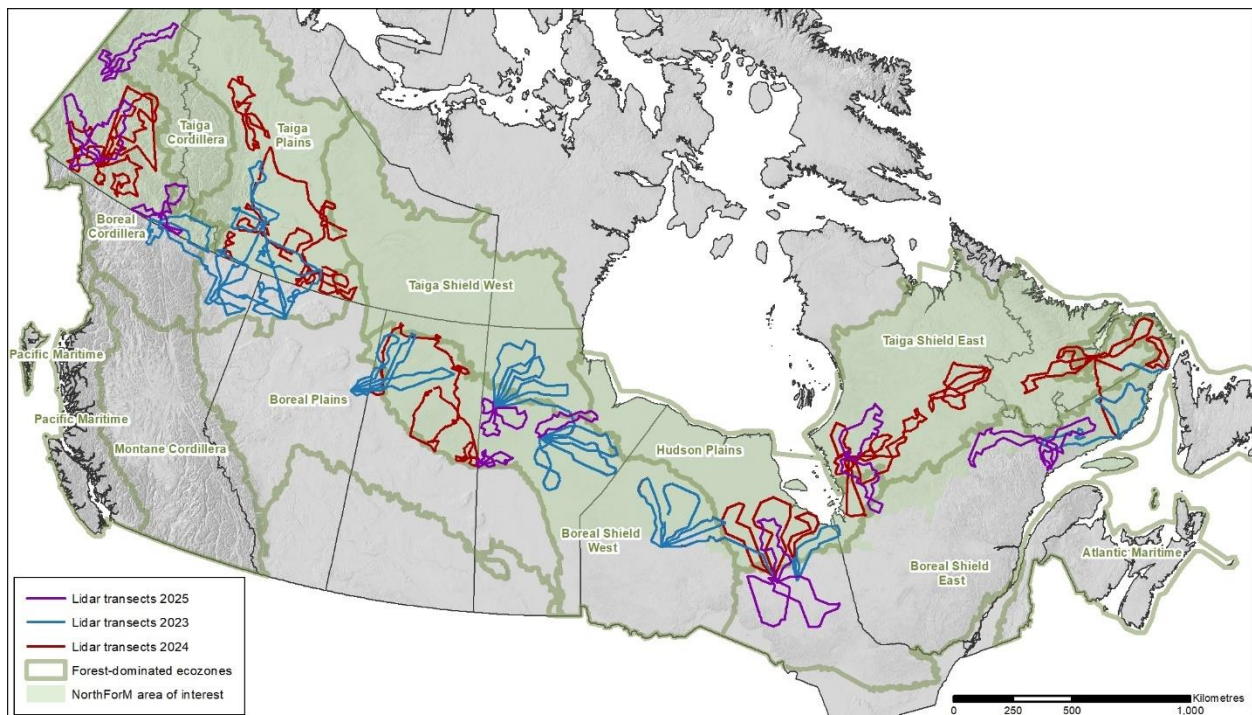
160

**Table 1. Summary of ALS acquisition specifications for the 2023-2025 acquisition program.**

Requirement	Acquisition 2023–2025
Aggregate nominal pulse density (ANDP)	12 pulses/m <sup>2</sup>
Aggregate nominal pulse spacing (ANPS)	0.29 m
Footprint diameter	0.30 m
Scan angle	+/-20 degrees on either side of nadir (40 degrees total field of view)
Horizontal datum	NAD 83 CSRS epoch 2010
Height reference	Vertical datum: CGVD 2013 Geoid model: CGG2013a
Map projection	Universal Transverse Mercator (UTM)
Pulse returns	Multiple
Classification	1 – Processed but unclassified 2 – Ground 3 – Low vegetation 4 – Medium vegetation 5 – High vegetation 7 – Low points (noise) 9 – Water 18 – High noise
Intensity Value	Normalized 16-bit values, according to the method described in the ASPRS LAS 1.4 R15 specification.
Data Format	LAS 1.4 R-15, Point data record format 6, compressed in LAZ
Swath width	500 m (2023) or 800 m (2024 and 2025)

161

162



163

164

165

166

**Figure 1. Airborne laser scanning (ALS) transects flown in 2023 (~20,000km), 2024 (~23,000 km), and 2025 (~12,000 km). The Northern Forest Mapping (NorthForM) acquisitions were largely focused on northern ecoregions to improve mapping in unmanaged forests.**

167 **Table 2. Airborne lidar vendors for acquisition years 2023,2024, and 2025. Each lidar plot (described in section 2.4) is**  
 168 **linked to acquisition information in a relational database.**

Acquisition year	Vendor	Lidar sensor
2023	Aeroquest Mapcon	Riegl VQ-1560II-S
	Eagle Mapping	Riegl VQ-780II-S & Riegl VQ-1560II-S
2024	Aeroquest Mapcon	Riegl VQ-1560 II-S
	Eagle Mapping	Riegl VQ-780II-S & Riegl VQ-1560II-S
	McElhanney	Leica TerrainMapper-2
2025	Aeroquest Mapcon	Riegl VQ-1560 II-S
	Kisik	Riegl VQ-1560 II -S

169

170

171

172 Canada’s National Forest Inventory (NFI) employs a systematic sampling strategy based upon 2 km x 2 km photo  
 173 plots established on a 20 x 20 km grid, with the intent to sample 1% of Canada’s landmass. The 20 x 20 km sample  
 174 grid is in turn nested within a 4 x 4 km system (Gillis et al., 2005). Candidate NorthForM ground plot locations were  
 175 selected using a stratified sampling strategy employing sampling units that combined ecozone (Figure 1), and  
 176 satellite-derived percent conifer and canopy closure obtained from the Spatialized Canadian National Forest  
 177 Inventory (Guindon et al., 2024). Ground plot locations were then selected using the NFI’s 4 x 4 km sampling  
 178 framework. Together, the NFI photo plot and NorthForM ground plot networks were used to guide ALS transect  
 179 design, with plot centres used as targets between which lidar data were acquired. Additional ALS transects were  
 180 established in an effort to obtain a balanced sample across northern forest-dominated ecozones where access was  
 181 possible (Figure 1).

182 **2.3 Data processing**

183 **2.3.1 Point cloud processing**

184 Following their delivery by the ALS vendors, subsequent processing of the point cloud data was performed using  
 185 LAStools (version 2.0.4; rapiddlasso GmbH). Footprint polygons were first created for each point cloud tile; the  
 186 footprints followed the exterior edges of ALS returns and captured large internal voids. Classified lidar point clouds  
 187 were then normalized to obtain heights above ground, with returns less than 0 m and greater than 100 m being  
 188 removed. Returns with scan angles exceeding 20 degrees or classified as high noise (class 18) were dropped from  
 189 the point clouds (Table 1). The point clouds were then reprojected from their universal transverse Mercator (UTM)  
 190 projections (Table 1) to a common national Lambert conformal conic projection employed by the NTEMS program  
 191 (Table 3). The normalized and reprojected point clouds were then used to calculate point cloud metrics.

192 **Table 3. Projection information for National Terrestrial Ecosystem Monitoring System (NTEMS) spatial data: a custom**  
 193 **Lambert conformal conic projection with two standard parallels using the NAD83 horizontal datum. Lidar plots were**  
 194 **generated using this projection.**

Projection information	Projected coordinate system	Lambert Conformal Conic 2SP
	Projection	Lambert conformal conic
	Authority	Custom
	Linear unit	Metre (1.0)
	False easting	0
	False northing	0
	Central meridian	-95.0 degrees
	Standard parallel 1	49.0 degrees
	Standard parallel 2	77.0 degrees
Geographic coordinate system information	Latitude of origin	49.0 degrees
	Geographic coordinate system	NAD 1983
	WKID	4269
	Authority	EPSG
	Angular unit	Degree (0.0174532925199433)
	Prime meridian	Greenwich (0.0)
	Horizontal datum	North American 1983
	Spheroid	GRS 1980
	Semimajor axis	6378137.0
Semiminor axis	6356752.314140356	
Inverse flattening	298.257222101	

195

### 196 2.3.2 Lidar plots and point cloud metrics

197 Lidar plots and the databases in which they are stored were created using Python and ESRI's ArcPy package. Lidar  
 198 plots were generated as point feature classes falling within the lidar transect swaths. Using the point cloud footprints,  
 199 lidar plots were located away from the edges of swaths and large interior voids to avoid areas of missing data. The  
 200 lidar plot centre coordinates aligned with the pixel centres of 30 m spatial resolution NTEMS raster products, which  
 201 use the NTEMS Lambert conformal conic projection (Table 3). Plots that fell within the NTEMS land cover  
 202 product's water class (Hermosilla et al., 2022) were removed. For each lidar plot, an individual 30 m x 30 point  
 203 cloud was then clipped from which area-based metrics would be calculated in subsequent steps.

204 Lidar point cloud metrics were calculated for each 30 m x 30 m lidar plot using the R packages lidR (Roussel et al.,  
 205 2020; Roussel and Auty, 2023) and lidRmetrics (Tompalski, 2024). As the final products are intended to inform a  
 206 variety of applications, including forest inventory, regeneration assessment, and wildfire fuels, the metrics were  
 207 generated in four groups using: (1) all returns above 0 m, (2) first returns above 0 m, (3) all returns above 2 m, and  
 208 (4) first returns above 2 m. Two height thresholds were used so that models could be created that either consider all  
 209 vegetation from the ground surface upwards (i.e.,  $\geq 0$  m), or with a focus on overstory structure ( $> 2$  m). Metrics  
 210 were calculated using only first returns as they have been shown to be more consistent than metrics based on all  
 211 returns (Bater et al., 2011); however, metrics considering all returns provide a more comprehensive characterization  
 212 of vertical forest structure and may be preferred for applications that consider more than just the upper canopy  
 213 (Singh et al., 2016). Each group included the same set of metrics, but values varied based on the combination of  
 214 height threshold (0 m or 2 m) and return type (all returns or first returns only). In total, 369 point cloud metrics were

215 generated; Table 4 categorizes these metrics by type (for a full list of metrics included in the database, see  
 216 Supplement A).

217 **Table 4. Types of point cloud metrics calculated from non-ground returns from ALS transects. In total, 369 metrics were**  
 218 **generated. Metrics were calculated for four groups of returns using: (1) all returns above 0 m, (2) first returns above 0 m,**  
 219 **(3) all returns above 2 m, and (4) first returns above 2 m. For a full list of metrics see Supplement A, and for detailed**  
 220 **descriptions see Tompalski (2024).**

Metric types	Description	Example metrics
Simple descriptive statistics	Basic statistical measures (e.g., mean, variance, skewness) summarizing point cloud height distribution (Bouvier et al., 2015; Lefsky et al., 2005; Nilsson, 1996).	zmean zsd_above2
Number of points by return number	Counts of ALS returns classified by return order.	n_return_1 n_return_4_above2
Number and proportion of returns by echo type	The count and relative frequency of returns categorized as single, first, intermediate, or last echoes.	n_last n_intermediate_above2
Height percentiles	Specific quantiles (e.g., 10th, 50th, 90th percentile) of the point cloud height distribution.	zq5 zq50_above2_first
Proportion of returns above threshold height	The fraction of returns exceeding a predefined height, used to characterize canopy cover (Solberg et al., 2006).	pzabove2 pzabovemean_first
Vertical structure	Metrics describing the distribution and variation of ALS returns along the vertical axis (van Ewijk et al., 2011; Shannon, 1948).	ziqr VCI_above2_first
Cumulative point density	The cumulative proportion of returns found in nine equal height intervals (Woods et al., 2008).	zpcum1 zpcum5_above2_first
L-moments metrics	Statistical measures capturing the shape of the height distribution, providing robust alternatives to conventional descriptive statistics (Frazer et al., 2011).	Lcoefvar L1_above2
Metrics based on leaf area density	Estimates of foliage distribution and density (Hopkinson et al., 2013; Magnussen and Boudewyn, 1998).	lad_mean lad_min_above2
Interval metrics	Metrics derived from predefined height intervals, summarizing point density at different canopy levels.	pz_1_2 pz_8_9_first
Rumple	A measure of canopy surface roughness or complexity based on the ratio of 3D to 2D surface area (Kane et al., 2010).	rumple rumple_above2_first
Metrics based on kernel density estimation	Metrics derived from smoothed height distributions (McGaughey, 2024).	kde_peak3_elev kde_peak2_diff_above2_first

221

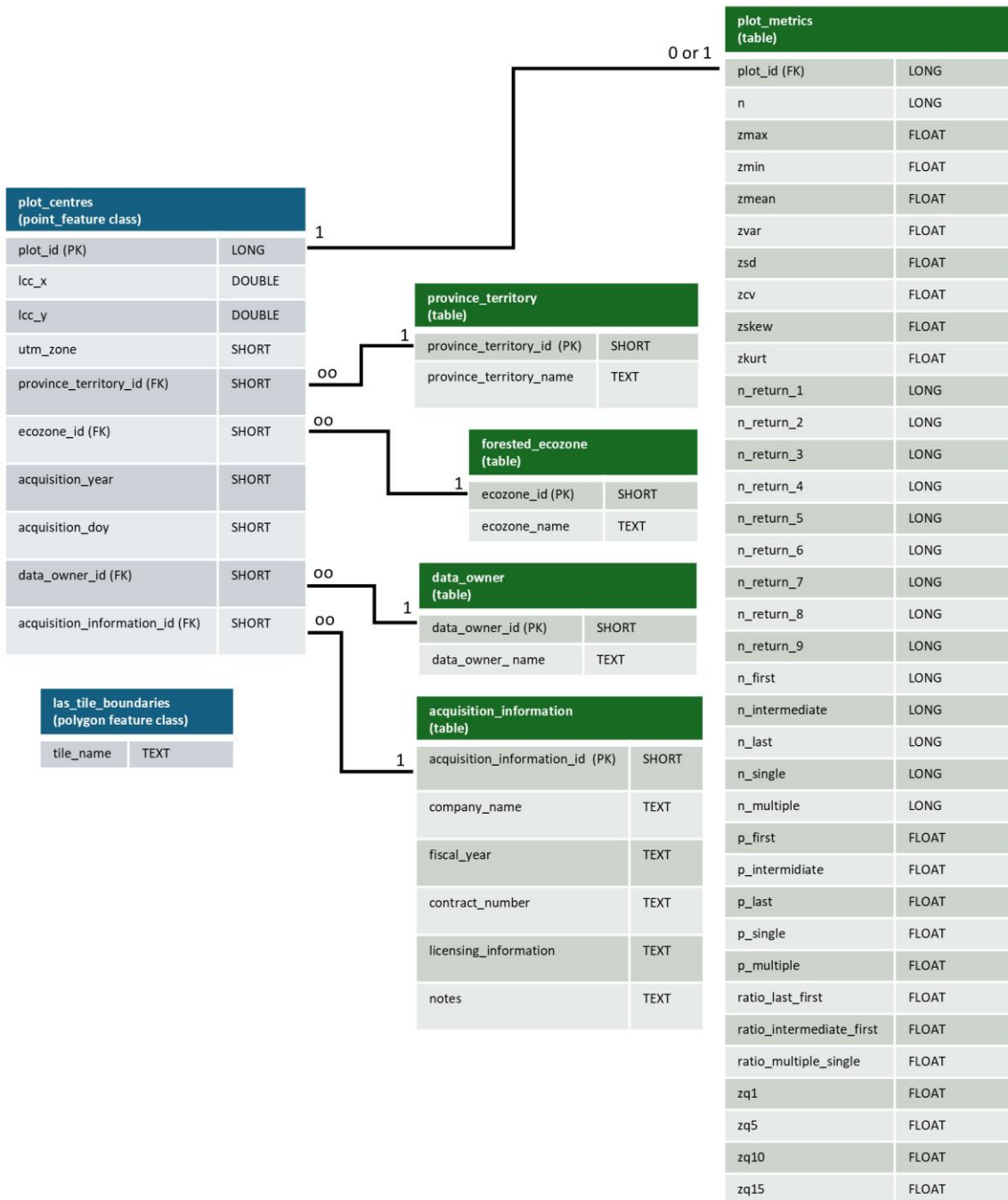
## 222 **2.4 Lidar plots database**

223 Lidar plots and associated point cloud metrics are distributed as SQLite GeoPackages<sup>1</sup>, which are an open and non-  
224 proprietary format. Each acquisition year (i.e., 2023, 2024, and 2025) will be stored in a separate database. Each  
225 GeoPackage contains a point feature class storing lidar plots on the NTEMS 30 m grid, a feature class delineating  
226 point cloud footprints, as well as a series of data tables storing point cloud metrics, province or territory, UTM zone,  
227 ecozone, and information related to individual acquisitions (Figure 2). Given the large number of metrics in the full  
228 database (Supplement A), for each year an abridged version of the dataset is also being shared that contains a subset  
229 of commonly used metrics for forest inventory (White et al., 2013, 2017a; Supplement B).

230

---

<sup>1</sup> <https://www.geopackage.org/>



\*Note: too many fields to list\*

231

232  
233  
234

Figure 2. Entity relationship diagram describing the structure of the lidar plots database. In total, the plot metrics table includes 369 point cloud metrics for each lidar plot, with an abridged version of the database available including a subset of 40 metrics.

235 **3 Results**

236 **3.1 ALS transects acquisitions**

237 A total of ~20,000 km, ~23,000 km, and ~12,000 km of ALS transect data were acquired in 2023, 2024, and 2025,  
238 respectively (Figure 1). The 2023 acquisition focused on collecting data over forest-dominated ecozones that are  
239 currently lacking ALS coverage (White et al., 2025). The 2023 ALS acquisitions were significantly impacted by  
240 smoke caused by unprecedented wildfire activity in Canada (Jain et al., 2024), and as a result, 5,000 km of planned  
241 acquisitions were postponed for capture in 2024. The 2024 and 2025 transects focused on acquiring data over  
242 NorthForM ground plots (Boucher et al., 2023). In 2025, wildfire activity and inclement weather resulted in only  
243 64% of planned data acquired. During the 2023, 2024, and 2025 field seasons over 900 ground plots were measured.  
244 Table 5 summarizes sampling intensity within NTEMS treed land cover classes for the 2023 acquisition (Hermosilla  
245 et al., 2022) by ecozone (Figure 1).

246

247 **Table 5. Sampling intensity within treed land cover classes by ecozone for 2023. “Land cover pixel area (ha)” represents**  
 248 **the area classified as a given land cover type within the ecozone (Figure 1). “Land cover pixel area (%)“ is the percent**  
 249 **coverage of a given land cover type in an ecozone. “Lidar plot area (ha)” represents the area of lidar plots within the**  
 250 **ecozone that falls within a given land cover type. “Sampling intensity (%)” is calculated as lidar plot area divided by pixel**  
 251 **area and multiplied by 100.**

Ecozone	Land cover class	Land cover pixel area (ha)	Land cover pixel area (%)	Lidar plot area (ha)	Sampling intensity (%)
Boreal Cordillera	Wetland-treed	656,907	1.5	2,609	0.3972
	Coniferous	21,292,772	47.9	79,718	0.3744
	Broadleaf	1,286,953	2.9	2,915	0.2265
	Mixedwood	729,463	1.6	1,113	0.1526
Boreal Plains	Wetland-treed	5,732,402	8.0	7,930	0.1383
	Coniferous	17,817,472	25.0	15,142	0.0850
	Broadleaf	13,063,662	18.3	5,860	0.0449
	Mixedwood	2,104,651	2.9	2,437	0.1158
Boreal Shield East	Wetland-treed	1,787,152	1.4	4,888	0.2735
	Coniferous	42,287,435	34.2	99,850	0.2361
	Broadleaf	8,328,982	6.7	2,115	0.0254
	Mixedwood	23,206,039	18.8	23,272	0.1003
Boreal Shield West	Wetland-treed	3,803,299	4.6	35,432	0.9316
	Coniferous	24,556,792	30.0	209,945	0.8549
	Broadleaf	2,946,598	3.6	8,100	0.2749
	Mixedwood	18,467,937	22.5	90,821	0.4918
Hudson Plains	Wetland-treed	13,322,381	30.6	27,665	0.2077
	Coniferous	2,970,087	6.8	10,084	0.3395
	Broadleaf	112,246	0.3	396	0.3526
	Mixedwood	1,107,734	2.5	5,939	0.5362
Taiga Plains	Wetland-treed	2,291,152	3.7	30,805	1.3445
	Coniferous	24,969,142	40.3	163,272	0.6539
	Broadleaf	2,721,976	4.4	28,823	1.0589
	Mixedwood	886,926	1.4	5,993	0.6757
Taiga Shield East	Wetland-treed	210,365	0.3	1	0.0005
	Coniferous	28,408,741	36.0	6,259	0.0220
	Broadleaf	192,614	0.2	1	0.0005
	Mixedwood	493,404	0.6	6	0.0012
Taiga Shield West	Wetland-treed	361,229	0.6	237	0.0656
	Coniferous	17,872,110	29.9	45,534	0.2548
	Broadleaf	865,552	1.4	1,441	0.1664
	Mixedwood	741,346	1.2	853	0.1151

252

### 253 3.1.2 Quality assurance results

254 Overall, the ALS acquisition specifications (Table 1) were met and often exceeded. A rare exception, however, were  
255 periodic changes in footprint sizes, swath widths, and point densities in areas with complex topography. These  
256 deviations are not unexpected and occur mostly in the mountainous areas of western Canada above the tree line, and  
257 impact less than one percent of the transect data.

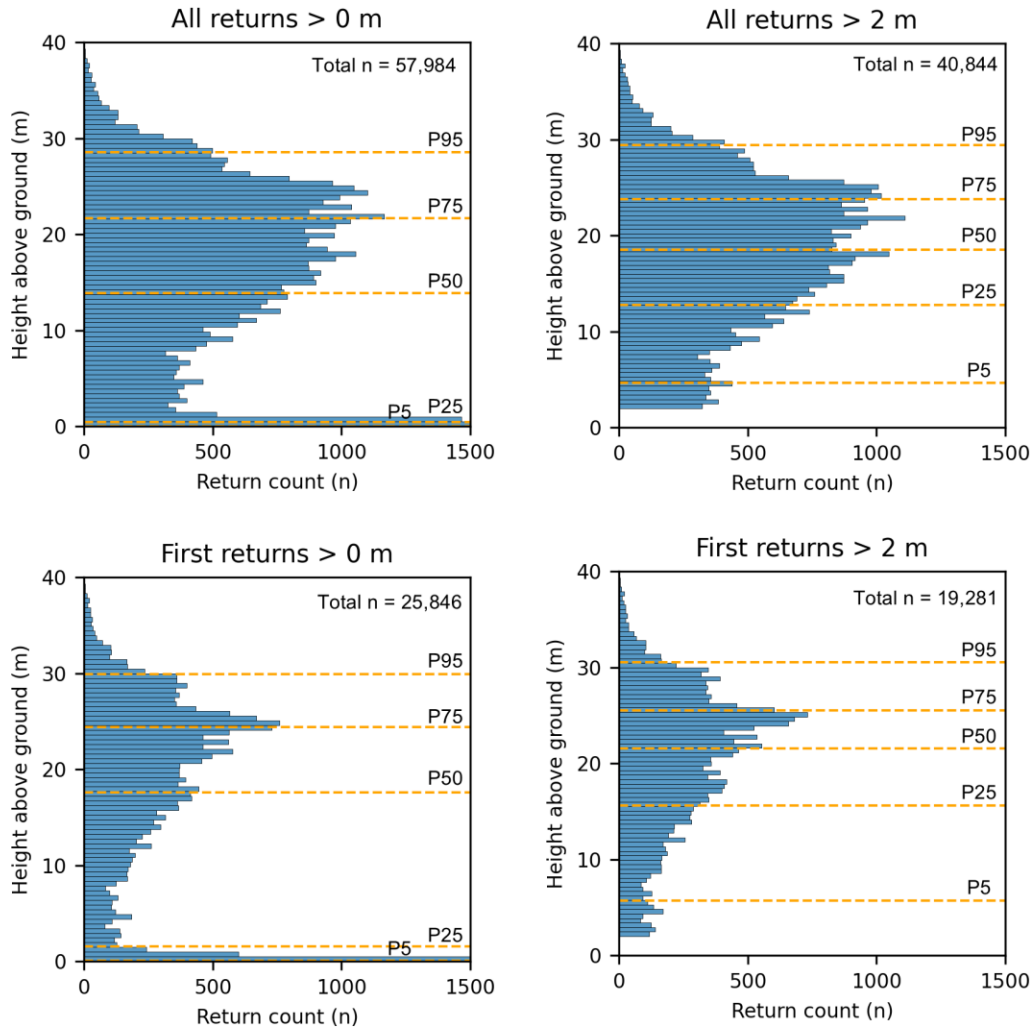
258 The ALS vendors (Table 2) corrected GNSS coordinates using PPP, with all reporting sub-metre horizontal and  
259 vertical accuracies. Point cloud classifications were validated following guidance in section 8.6 of the Canadian lidar  
260 acquisition standards (CSA Group, 2025), which indicate that point classifications should be consistent across the  
261 entire project with minimal variations in the classification quality between tiles or swaths. For each acquisition year,  
262 twenty 1 km x 1 km point cloud tiles distributed across the acquisition areas (Figure 1) were selected for analysis.  
263 Within each tile, 20 randomly selected 400 m<sup>2</sup> areas were then clipped and three-dimensional visual checks of the  
264 point cloud classifications were performed using FUSION's pdq viewer (McGaughey, 2024). All point clouds were  
265 rasterized based on return class (Table 1) and hillshades were generated from the DTMs. Raster surfaces were then  
266 visually inspected to ensure specifications were met (e.g., all points were classified (unless withheld), water was  
267 properly classified, no areas with few or no ground returns, noise was classified correctly, DTMs were representative  
268 of the bare-Earth surface). Similarly, return counts and scan angles were rasterized to ensure transects fell within the  
269 specifications for point densities and swath widths (Table 1). All raster products were generated using LAStools  
270 (version 2.0.4). Any issues found were reported to the ALS data vendors who then made corrections.

### 271 3.2 Lidar plots databases

272 For the 2023 ALS transects, 15,353,866 lidar plots were generated within the lidar swaths. The full database  
273 including 369 point cloud metrics is 60.2 GB in size, and the abridged version of the database containing a subset of  
274 40 metrics is 7.2 GB. Both versions are shared as SQLite GeoPackages.

### 275 3.3 Point cloud metrics

276 Point cloud metrics were processed in four groups using: (1) all returns above 0 m, (2) first returns above 0 m, (3) all  
277 returns above 2 m, and (4) first returns above 2 m. Figure 3 shows an example of the four processing groups from  
278 the same lidar plot. The number of returns range from 19,281 (first returns > 2m) to 57,984 (all returns > 0m), while  
279 the height percentiles change by varying degrees between each group. The lower height percentiles are most  
280 sensitive to changes in height threshold, with the first return P5 changing from 0.06 m (0 m threshold) to 5.71m (2 m  
281 threshold), while P95 changes from 29.91 m (0 m threshold) to 30.55 m (2 m threshold).



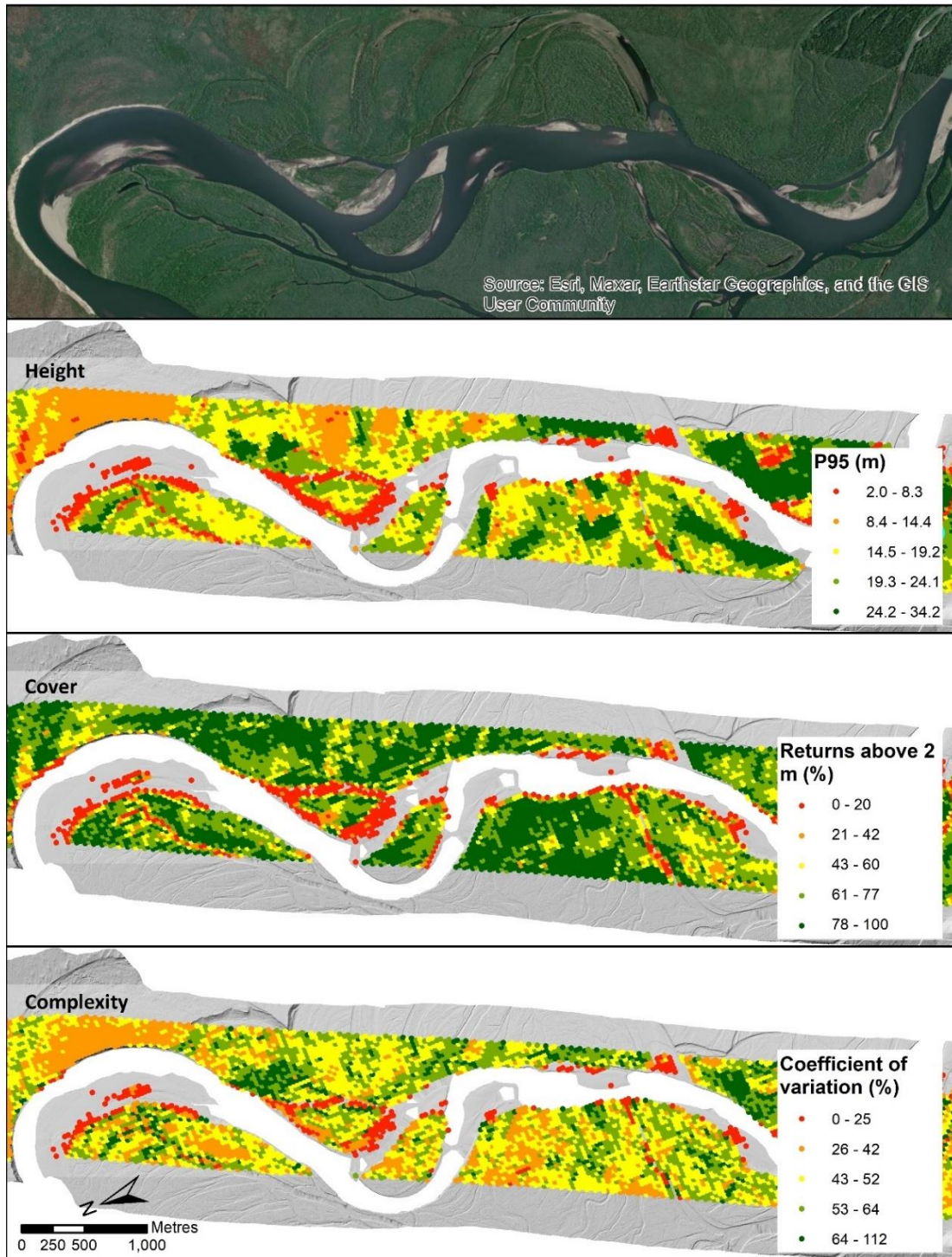
282

283 **Figure 3. Comparison of vertical distributions of returns from four different processing groups for the same lidar plot: all**  
 284 **returns above 0 m, all returns above 2 m, first returns above 0 m, and first returns above 2 m. P95 = 95<sup>th</sup> height**  
 285 **percentile, P75 = 75<sup>th</sup> height percentile, and so on. The plot is located along the Prophet River in northern British**  
 286 **Columbia (58° 17' 19" N, 122° 52' 30" W).**

287

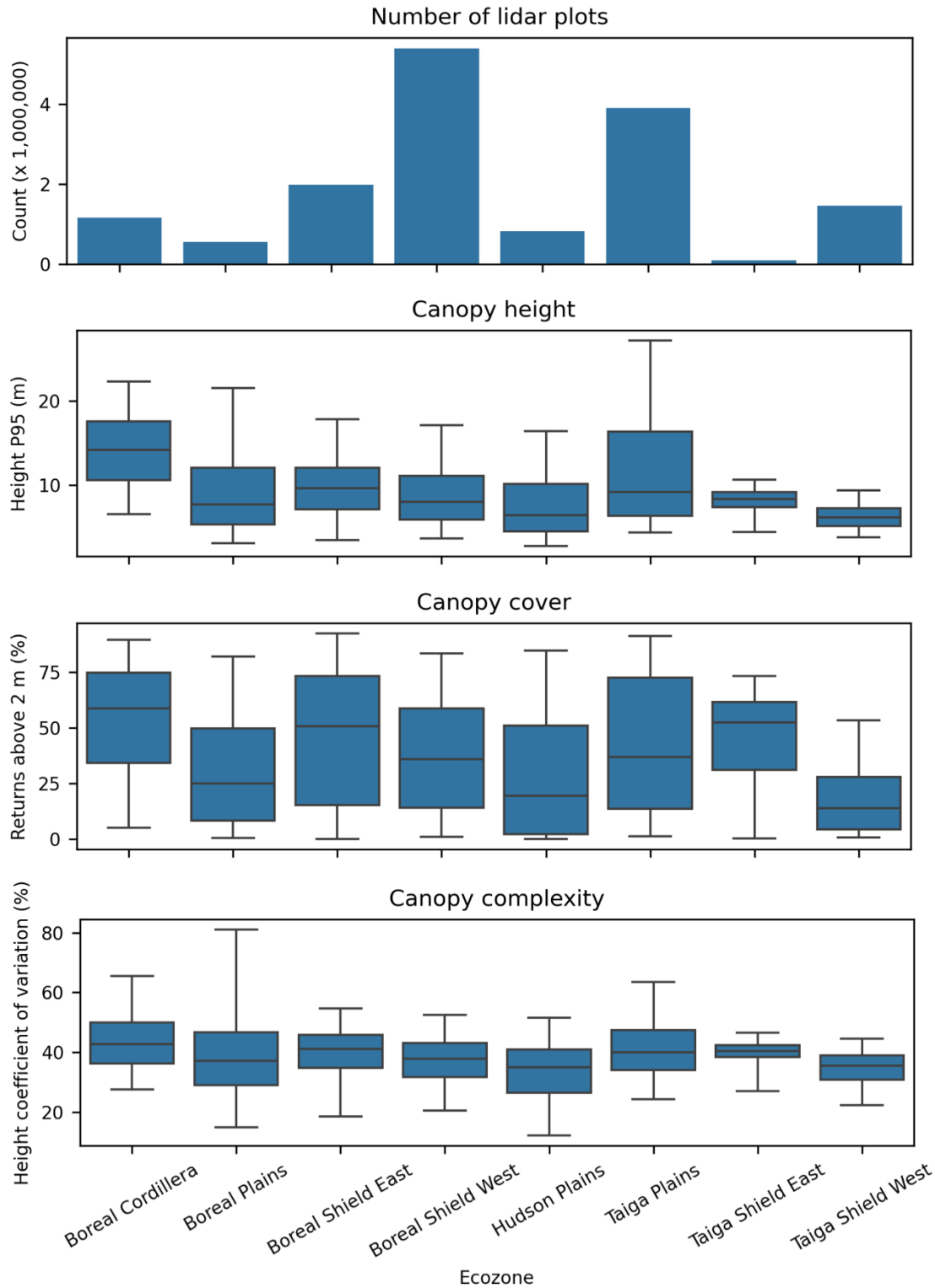
288 Fundamentally, lidar characterizes vegetation height, vertical structure, and cover (Li et al., 2008). Figure 4 shows  
 289 examples of lidar plots with point cloud metrics related to these attributes along a reach of the Liard River in  
 290 Northern British Columbia. Figure 5 provides summaries of height, cover and structure by ecozone for all 2023 lidar  
 291 plots.

292



293

294 Figure 4. Examples of lidar plot metrics, including: canopy height based on the 95th height percentile of first returns  
 295 greater than 2 m; canopy cover based on the proportion of first returns greater than 2 m; and canopy complexity based  
 296 on the coefficient of variation of first returns heights greater than 2m. The image in the top panel extends beyond the ALS  
 297 swath for added landscape context. The digital terrain model hillshade was derived from ALS returns with scan angles in  
 298 excess of 20 degrees, while lidar plots are limited to returns with scan angles less than or equal to 20 degrees (Table 1).  
 299 Data are located along the Liard River in northern British Columbia (59° 53' 22" N, 128° 19' 3" W).

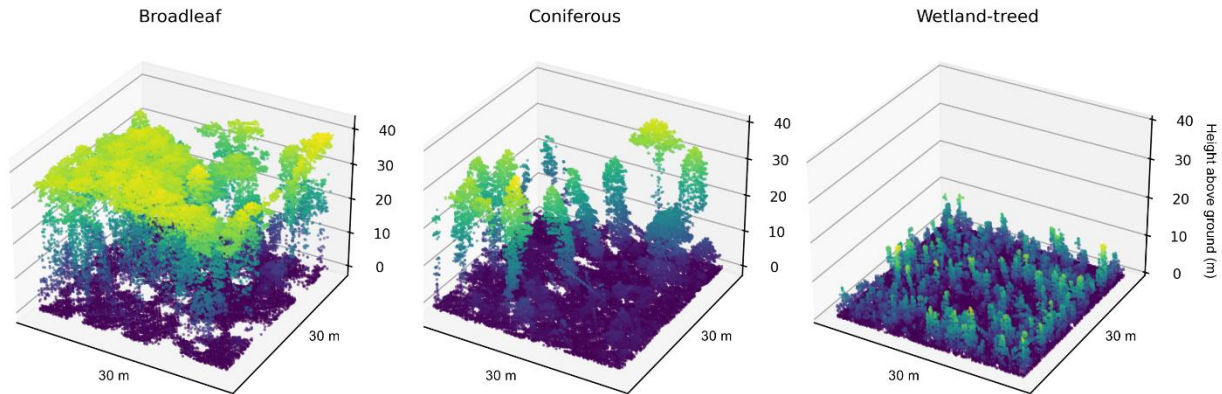


300

301 **Figure 5: Summary of vegetation metrics by ecozone (Figure 1) for the 2023 acquisition (total n = 15,353,866 lidar plots).**  
 302 **For the box and whisker plots, the box represents the interquartile range with the centre line showing the median, while**  
 303 **the whiskers represent the 5<sup>th</sup> and 95<sup>th</sup> percentiles.**

304 **3.3.1 Comparison of lidar plots with NTEMS satellite information products**

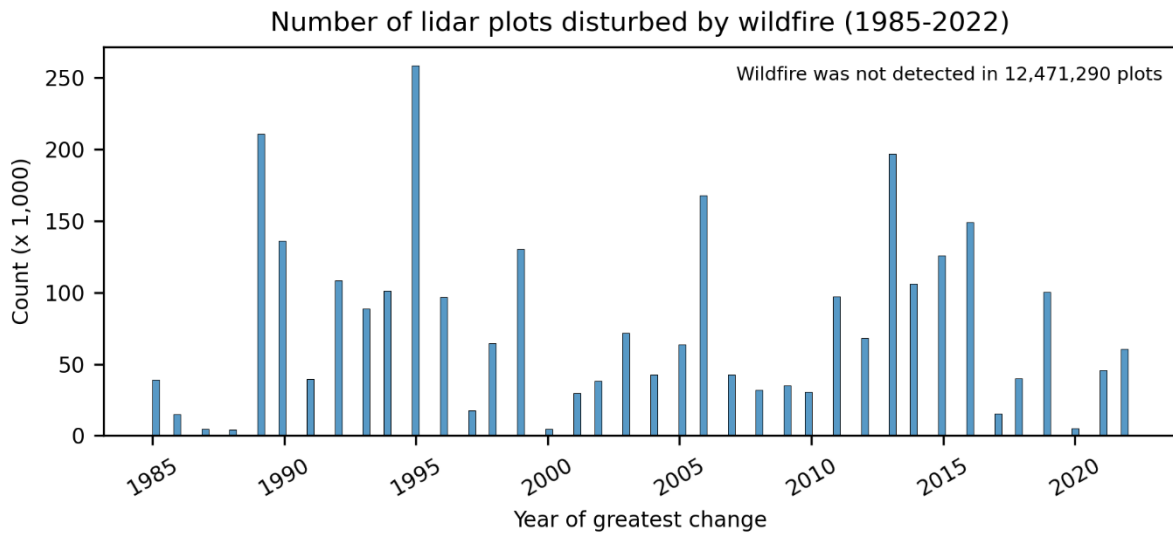
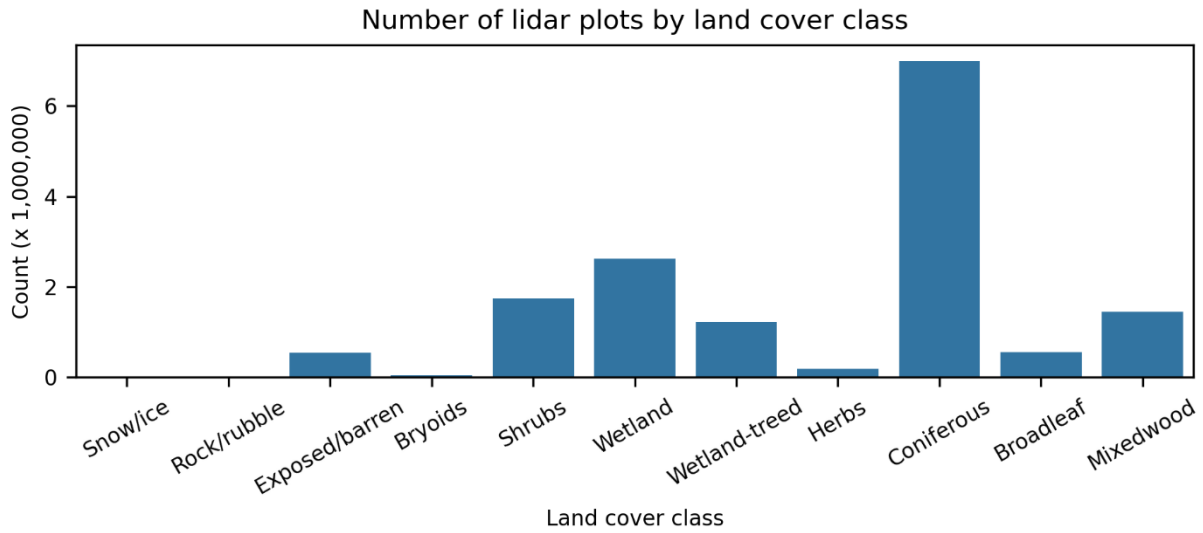
305 The NTEMS project provides a number of satellite-derived products characterizing forest-dominated ecozones,  
306 including land cover (Hermosilla et al., 2022) and recent wildfire disturbance history (Hermosilla et al., 2016).  
307 Figure 6 provides examples of point clouds clipped to lidar plots in three different treed land cover types. The  
308 broadleaf and coniferous plots are located in productive riparian stands, while the wetland-treed plot is located in a  
309 nearby treed bog or fen.



310  
311 **Figure 6. Examples of point clouds within lidar plots for three different treed land cover types. The plots are located along**  
312 **the Prophet River in northern British Columbia (58° 17' 19" N, 122° 52' 30" W).**

313  
314 Figure 7 provides distributions of 2023 lidar plots for land cover and year of recent wildfire disturbance (1985 -  
315 2022). For the 15,353,866 plots, the dominant land cover type (Hermosilla et al., 2022), excluding water within the  
316 plots, was coniferous (46%), followed by wetland (17%), shrubs (11%), mixedwood (9%), wetland-treed (8%),  
317 broadleaf (4%), exposed/barren land (3%), herbs (1%), bryoids (0.3%), rock/rubble (0.04%), and snow/ice  
318 (0.001%). Moreover, 19% were disturbed by wildfire (Hermosilla et al., 2016) between 1985 and 2022 (Figure 7).

319  
320



321

322

323

Figure 7. Comparison between lidar plots and multidecadal NTEMS satellite information products, including land cover class (excluding water) and number of plots disturbed by wildfire between 1985 and 2022 (Hermosilla et al., 2016; 2022).

## 324 4 Discussion

325 The ALS transects, lidar plots, and point cloud metrics presented here represent a comprehensive and coordinated  
326 effort to sample forest structure in Canada’s unmanaged northern forests. By collecting high-density ALS data  
327 across ecologically diverse regions that lack structural information, this dataset fills a critical gap in the national  
328 forest monitoring landscape. The design and implementation of the acquisitions can address both scientific and  
329 operational needs, with particular relevance to wildfire fuel mapping (Andersen et al., 2005; Martin-Ducup et al.,  
330 2025; Riaño et al., 2003), forest inventory (Reutebuch et al., 2005; Wulder et al., 2008), carbon accounting  
331 (Andersen et al., 2011; Babcock et al., 2018), and ecosystem monitoring (Bolton et al., 2015; Matasci et al., 2018b).  
332 Open datasets allow fire researchers and other specialists unfamiliar with ALS point cloud processing to access these  
333 data in an analysis-ready and easy-to-use format. We chose to package the data as SQLite GeoPacackages, using  
334 vector feature classes to store spatial data. The aim is to ensure that the data are readily accessible and easy to use  
335 for those familiar with geographic information systems or scientific programming languages such as Python, R or  
336 Julia. While ALS derivatives are typically distributed using raster formats (e.g. Assmann et al., 2022; Shi et al.,  
337 2025), the layout of the transects (Figure 1) would result in raster surfaces consisting largely of “no data” values.  
338 Should a user desire, the point feature classes can be easily rasterized for inclusion in an analysis workflow requiring  
339 gridded surfaces. For users interested in leveraging NTEMS datasets (e.g. Hermosilla et al., 2022, 2024; Matasci et  
340 al., 2018a, b), the lidar plots will integrate seamlessly as all data share a common spatial resolution, projection  
341 (Table 3), and origin coordinates. Should users prefer to generate metrics at other spatial resolutions, the raw ALS  
342 point cloud data will also be made publicly available.

343 A key advantage of this dataset lies in its flexibility. The inclusion of point cloud metrics from the four combinations  
344 of return types and height thresholds (all returns and first returns,  $> 0$  m and  $> 2$  m) supports diverse modeling  
345 approaches, including forest inventory, regeneration assessment, and canopy fuel characterization (Table 4, Figure 3,  
346 Supplement A, Supplement B). For those focused on developing forest inventories, point cloud metrics based on  
347 returns above 2 m, which remove the effects of shrubs and small trees, may be the most appropriate. For users  
348 interested in forest regeneration or fuels attributes such as canopy base height, retaining lower returns may be  
349 beneficial (Arumäe and Lang, 2018; Naesset, 2011; Stefanidou et al., 2020). The decision to use first returns or all  
350 returns may be guided by examining performance diagnostics from predictive models (Arumäe and Lang, 2018;  
351 Bater et al., 2011). White et al. (2013, 2017a) provide advice on model development for enhanced forest inventories,  
352 and the methods described and citations therein can inform a wide range of applications related to ALS and ecology.

353 The value of lidar plots lies in their role as a scalable intermediary between field measurements and satellite-based  
354 inventories, effectively increasing the sample size of required model inputs (Wulder et al. 2012b). When integrated  
355 with ground plots and satellite data, lidar plots can enable the generation of wall-to-wall maps of forest attributes  
356 such as height, volume, and biomass. This approach has been demonstrated nationally for Canada’s forests using  
357 previously acquired ALS transects (Matasci et al., 2018a, b) and the expansion of this sampling framework with the  
358 new acquisitions described herein substantially increases coverage across previously unsampled areas.

359 Despite the aforementioned strengths of lidar plots, several aspects of these data warrant further consideration. In  
360 particular, the ALS acquisitions are largely restricted to northern forests (Figure 1). Given the focused sampling to  
361 these northern forests, conditions present in the southern extent of Canada's forests will not be captured, as  
362 exemplified by the distributions of land cover classes within lidar plots (Figure 7), which differ markedly from the  
363 national summaries reported by Hermosilla et al. (2022). As these lidar transects were specifically designed to  
364 characterize northern forest conditions, they would need to be augmented with ALS data from southern forests to  
365 enable the development of national models of forest structure, as demonstrated in Matasci et al. (2018b). With more  
366 than 70% of Canada's managed forest area in the south having ALS data available (White et al., 2025), additional  
367 samples of ALS are readily available. Sampled transects also inhabit an unfamiliar form and scale for most users of  
368 ALS data. Within the lidar plots can be found detailed characterizations of both vegetation structure and terrain  
369 morphology (Figure 4, Figure 6). The data can also be analyzed at regional scales, by pooling lidar plots (Figure 5)  
370 to contribute to population estimates of attributes such as volume or biomass (Andersen et al., 2011; Margolis et al.,  
371 2015). However, by design transect data alone are not spatially exhaustive, precluding independent wall-to-wall  
372 mapping, and are intended to be incorporated with satellite and other ancillary data to support mapping via  
373 modelling methods such as imputation (Coops et al., 2021).

374 One of the objectives of the NorthForM program is the collection of coincident ALS and ground plot data. As the  
375 program progresses, GNSS locations from ground plots will be used to clip ALS point clouds to the plot extents. The  
376 same suite of 369 metrics described above (Table 4, Supplement A) will then be generated for the ground plots and  
377 made available. In combination, the forest inventory measurements made in situ within ground plots, ground plot  
378 point cloud metrics, and the lidar plot point cloud metrics will be powerful datasets for the spatially explicit  
379 predictive modelling of forest structure (Matasci et al., 2018a, b; Zald et al., 2016).

380 These data will be used for a number of initiatives. Wildfire specialists will employ the data to contribute to the  
381 development of predictive models that estimate fuel attributes such as canopy species composition, crown base  
382 height, crown bulk density, forest floor cover type, and litter load (Boucher et al., 2023). National models of forest  
383 inventory attributes will be improved and brought up-to-date, including those related to height, structural  
384 complexity, biomass, and volume (Matasci et al., 2018b). The data will also inform carbon accounting by  
385 contributing to the development of pixel-based biomass yield curves (Tompalski et al., 2025).

386 Beyond Canada, the ALS transect network provides an example for characterizing vegetation structure over large  
387 areas at a relatively low cost. The transects-based approach offers a transferable framework for designing national  
388 forest monitoring programs in countries where consistent, high spatial resolution structural data are lacking. By  
389 linking ALS measurements to ground plots and satellite observations, the dataset can support regional to global  
390 assessments of carbon stocks, disturbance dynamics, and climate-driven change.

391 Herein we focus largely on point cloud metrics derived from ALS data acquired in 2023; however, data collected in  
392 2024 and 2025 will be made available following the same processing stream and use the same basic database  
393 schema described herein. The addition of terrain metrics (e.g. height, slope, curvature, solar radiation) is underway

394 and will be included as an additional table in future releases. The raw ALS point cloud data will also be made  
395 publicly available.

## 396 **5 Data availability**

397 The 2023 lidar plots and point cloud metrics described here are available at  
398 <https://doi.org/10.5281/zenodo.16782860> on Zenodo (Bater et al., 2025).

399 The 2023 data and collections from subsequent acquisition years collected under the same monitoring framework  
400 will be released as independent datasets and will share a common structure and repository. They will be made  
401 available through Canada's National Forest Information System (NFIS) at: [https://opendata.nfis.org/mapserver/nfis-](https://opendata.nfis.org/mapserver/nfis-change_eng.html)  
402 [change\\_eng.html](https://opendata.nfis.org/mapserver/nfis-change_eng.html)

403 The most current versions of the metrics databases and raw ALS point clouds will be made findable through NFIS.

## 404 **6 Conclusion**

405 The lidar plots and point cloud metrics described herein form part of an open-data initiative to enhance structural  
406 information on Canada's northern forests. By sampling remote and underrepresented forest-dominated ecozones,  
407 this dataset supports key applications in wildfire risk assessment, forest inventory, and ecosystem monitoring. These  
408 data offer a scalable foundation for integrating field and satellite observations to inform national mapping and  
409 monitoring efforts, helping address long-standing data gaps in Canada's forest information landscape. In  
410 combination with similar lidar plots representing conditions in southern Canada, these data form a key input towards  
411 updating and improving the structural data layers (e.g., biomass, canopy height and cover) delivered via the National  
412 Terrestrial Ecosystem Monitoring System. The inclusion of a wide range of metrics provides flexibility for diverse  
413 predictive modeling needs, while the database structure ensures usability by researchers and practitioners who may  
414 not be well-versed in remote sensing.

## 415 **Author contribution**

416 Conceptualization by MW, JW, TH, and CB. Data curation by CB. Formal analysis by CB. Methodology by JW, CB,  
417 HC, and PT. Software by CB, HC, and PT. Supervision by MW, JW, and TH. Writing by CB, MW, JW, TH, and PT..

## 418 **Competing interests**

419 The contact author has declared that neither they nor their co-authors have any competing interests.

## 420 **Acknowledgements**

421 The ALS data were acquired with funding from the Canadian Forest Service's Northern Forest Mapping  
422 (NorthForM) program, which aims to enhance mapping of Canada's northern forests, identify wildfire hazards, and  
423 support community wildfire resilience and mitigation measures.

424 We thank Jonathan Boucher (Canadian Forest Service, Laurentian Forestry Centre) for his invaluable insights into  
425 the next generation of the Canadian Forest Fire Danger Rating System and how remote sensing data can support  
426 future fire behaviour models.

## 427 **References**

- 428 Aldred, A. and Bonnor, G. M.: Application of airborne lasers to forest surveys, Canadian Forestry Service,  
429 Petawawa National Forestry Centre. 62p, 1985.
- 430 Andersen, H. E., McGaughey, R. J., and Reutebuch, S. E.: Estimating forest canopy fuel parameters using LIDAR  
431 data, *Remote Sens. Environ.*, 94, 441–449, <https://doi.org/10.1016/j.rse.2004.10.013>, 2005.
- 432 Andersen, H. E., Strunk, J., and Temesgen, H.: Using airborne light detection and ranging as a sampling tool for  
433 estimating forest biomass resources in the upper Tanana Valley of interior Alaska, *West. J. Appl. For.*, 26, 157–164,  
434 <https://doi.org/10.1093/wjaf/26.4.157>, 2011.
- 435 Arumäe, T. and Lang, M.: Estimation of canopy cover in dense mixed-species forests using airborne lidar data, *Eur.*  
436 *J. Remote Sens.*, 51, 132–141, <https://doi.org/10.1080/22797254.2017.1411169>, 2018.
- 437 Assmann, J. J., Moeslund, J. E., Treier, U. A., and Normand, S.: EcoDes-DK15: High-resolution ecological  
438 descriptors of vegetation and terrain derived from Denmark’s national airborne laser scanning data set, *Earth Syst.*  
439 *Sci. Data*, 14, 823–844, <https://doi.org/10.5194/essd-14-823-2022>, 2022.
- 440 Babcock, C., Finley, A. O., Andersen, H. E., Pattison, R., Cook, B. D., Morton, D. C., Alonzo, M., Nelson, R.,  
441 Gregoire, T., Ene, L., Gobakken, T., and Næsset, E.: Geostatistical estimation of forest biomass in interior Alaska  
442 combining Landsat-derived tree cover, sampled airborne lidar and field observations, *Remote Sens. Environ.*, 212,  
443 212–230, <https://doi.org/10.1016/j.rse.2018.04.044>, 2018.
- 444 Bater, C., White, J., Chen, H., Tompalski, P., Hermosilla, T., and Wulder, M.: Lidar plots and point cloud metrics  
445 derived from airborne laser scanning transects acquired over forests in northern Canada., *Zenodo*,  
446 <https://doi.org/10.5281/zenodo.16782860>, 2025.
- 447 Bater, C. W., Wulder, M. A., Coops, N. C., Nelson, R. F., Hilker, T., and Nasset, E.: Stability of sample-based  
448 scanning-LiDAR-derived vegetation metrics for forest monitoring, *IEEE Trans. Geosci. Remote Sens.*, 49, 2385–  
449 2392, <https://doi.org/10.1109/TGRS.2010.2099232>, 2011.
- 450 Bolton, D. K., Coops, N. C., and Wulder, M. A.: Characterizing residual structure and forest recovery following  
451 high-severity fire in the western boreal of Canada using Landsat time-series and airborne lidar data, *Remote Sens.*  
452 *Environ.*, 163, 48–60, <https://doi.org/10.1016/j.rse.2015.03.004>, 2015.
- 453 Boucher, J., Cotton-Gagnon, A., Zerb, J., Smiley, B. P., Russo, G., and Nolan, M.: Field guide: sampling fuels in the  
454 context of the Next-Generation Canadian Forest Fire Danger Rating System (NG-CFFDRS). *Field Sampling*

455 Protocol and List of Attributes for Field Crews (2023), 26 pp., 2023.

456 Bourdeau-Goulet, S. and Hassanzadeh, E.: Comparisons between CMIP5 and CMIP6 models: simulations of climate  
457 indices influencing food security, infrastructure resilience, and human health in Canada, *Earth's Futur.*, 9,  
458 e2021EF001995, <https://doi.org/https://doi.org/10.1029/2021EF001995>, 2021.

459 Bouvier, M., Durrieu, S., Fournier, R. A., and Renaud, J. P.: Generalizing predictive models of forest inventory  
460 attributes using an area-based approach with airborne LiDAR data, *Remote Sens. Environ.*, 156, 322–334,  
461 <https://doi.org/10.1016/j.rse.2014.10.004>, 2015.

462 Brandt, J. P.: The extent of the North American boreal zone, *Environ. Rev.*, 17, 101–161,  
463 <https://doi.org/10.1139/A09-004>, 2009.

464 Burton, P. J.: Understanding spring wildfires in Canada's northern forests, *Glob. Chang. Biol.*, 29, 5983–5985,  
465 <https://doi.org/10.1111/gcb.16879>, 2023.

466 Canadian Forest Service Fire Danger Group: An overview of the next generation of the Canadian Forest Fire Danger  
467 Rating System (Information Report GLC-X-26)., 70 pp., 2021.

468 Coops, N. C., Tompalski, P., Goodbody, T. R. H., Queinnec, M., Luther, J. E., Bolton, D. K., White, J. C., Wulder,  
469 M. A., van Lier, O. R., and Hermosilla, T.: Modelling lidar-derived estimates of forest attributes over space and  
470 time: A review of approaches and future trends, *Remote Sens. Environ.*, 260, 112477,  
471 <https://doi.org/10.1016/j.rse.2021.112477>, 2021.

472 Crowley, M. A., Stockdale, C. A., Johnston, J. M., Wulder, M. A., Liu, T., McCarty, J. L., Rieb, J. T., Cardille, J.  
473 A., and White, J. C.: Towards a whole-system framework for wildfire monitoring using Earth observations, *Glob.*  
474 *Chang. Biol.*, 29, 1423–1436, <https://doi.org/10.1111/gcb.16567>, 2023.

475 CSA Group: Airborne lidar data acquisition, 83 pp., <https://www.csagroup.org/store/product/2431645/>, 2025.

476 van Ewijk, K. Y., Treitz, P. M., and Scott, N. A.: Characterizing forest succession in central Ontario using lidar-  
477 derived indices, *Photogramm. Eng. Remote Sensing*, 77, 261–269, <https://doi.org/0099-1112>.  
478 DOI:10.1117/12.2223586, 2011.

479 Fassnacht, F. E., White, J. C., Wulder, M. A., and Næsset, E.: Remote sensing in forestry: current challenges,  
480 considerations and directions, *For. An Int. J. For. Res.*, 97, 11–37, <https://doi.org/10.1093/forestry/cpad024>, 2024.

481 Frazer, G. W., Magnussen, S., Wulder, M. A., and Niemann, K. O.: Simulated impact of sample plot size and co-  
482 registration error on the accuracy and uncertainty of LiDAR-derived estimates of forest stand biomass, *Remote*  
483 *Sens. Environ.*, 115, 636–649, <https://doi.org/10.1016/j.rse.2010.10.008>, 2011.

484 Gillis, M. D., Omule, A. Y., and Brierley, T.: Monitoring Canada's forests: The National Forest Inventory, *For.*  
485 *Chron.*, 81, 214–221, <https://doi.org/10.5558/tfc81214-2>, 2005.

486 Guindon, L., Manka, F., Correia, D. L. P., Villemaire, P., Smiley, B., Bernier, P., Gauthier, S., Beaudoin, A.,  
487 Boucher, J., and Boulanger, Y.: A new approach for Spatializing the Canadian National Forest Inventory (SCANFI)  
488 using Landsat dense time series, *Can. J. For. Res.*, 2010, <https://doi.org/10.1139/cjfr-2023-0118>, 2024.

489 Hansen, M. C., Egorov, A., Potapov, P. V., Stehman, S. V., Tyukavina, A., Turubanova, S. A., Roy, D. P., Goetz, S.  
490 J., Loveland, T. R., Ju, J., Kommareddy, A., Kovalskyy, V., Forsyth, C., and Bents, T.: Monitoring conterminous  
491 United States (CONUS) land cover change with Web-Enabled Landsat Data (WELD), *Remote Sens. Environ.*, 140,  
492 466–484, <https://doi.org/10.1016/j.rse.2013.08.014>, 2014.

493 Haslem, A., Kelly, L. T., Nimmo, D. G., Watson, S. J., Kenny, S. A., Taylor, R. S., Avitabile, S. C., Callister, K. E.,  
494 Spence-Bailey, L. M., Clarke, M. F., and Bennett, A. F.: Habitat or fuel? Implications of long-term, post-fire  
495 dynamics for the development of key resources for fauna and fire, *J. Appl. Ecol.*, 48, 247–256,  
496 <https://doi.org/10.1111/j.1365-2664.2010.01906.x>, 2011.

497 Hermosilla, T., Wulder, M. A., White, J. C., Coops, N. C., Hobart, G. W., and Campbell, L. B.: Mass data  
498 processing of time series Landsat imagery: pixels to data products for forest monitoring, *Int. J. Digit. Earth*, 9, 1035–  
499 1054, <https://doi.org/10.1080/17538947.2016.1187673>, 2016.

500 Hermosilla, T., Wulder, M. A., White, J. C., and Coops, N. C.: Land cover classification in an era of big and open  
501 data: Optimizing localized implementation and training data selection to improve mapping outcomes, *Remote Sens.*  
502 *Environ.*, 268, 112780, <https://doi.org/10.1016/j.rse.2021.112780>, 2022.

503 Hermosilla, T., Wulder, M. A., White, J. C., Coops, N. C., Bater, C. W., and Hobart, G. W.: Characterizing long-  
504 term tree species dynamics in Canada’s forested ecosystems using annual time series remote sensing data, *For. Ecol.*  
505 *Manage.*, 572, 122313, <https://doi.org/10.1016/j.foreco.2024.122313>, 2024.

506 Hopkinson, C., Wulder, M. A., Coops, N. C., Milne, T., Fox, A., and Bater, C. W.: Airborne lidar sampling of the  
507 Canadian boreal forest: planning, execution, and initial processing., in: *Proceedings of the SilviLaser 2011*  
508 *Conference*, 2011.

509 Hopkinson, C., Lovell, J., Chasmer, L., Jupp, D., Kljun, N., and van Gersel, E.: Integrating terrestrial and airborne  
510 lidar to calibrate a 3D canopy model of effective leaf area index, *Remote Sens. Environ.*, 136, 301–314,  
511 <https://doi.org/10.1016/j.rse.2013.05.012>, 2013.

512 Jain, P., Barber, Q. E., Taylor, S. W., Whitman, E., Castellanos Acuna, D., Boulanger, Y., Chavardès, R. D., Chen,  
513 J., Englefield, P., Flannigan, M., Girardin, M. P., Hanes, C. C., Little, J., Morrison, K., Skakun, R. S., Thompson, D.  
514 K., Wang, X., and Parisien, M.: Drivers and impacts of the record-breaking 2023 wildfire season in Canada, *Nat.*  
515 *Commun.*, 15, 6764, <https://doi.org/10.1038/s41467-024-51154-7>, 2024.

516 Kane, V. R., Bakker, J. D., McGaughey, R. J., Lutz, J. A., Gersonde, R. F., and Franklin, J. F.: Examining conifer  
517 canopy structural complexity across forest ages and elevations with LiDAR data, *Can. J. For. Res.*, 40, 774–787,  
518 <https://doi.org/http://www.nrcresearchpress.com/doi/abs/10.1139/X10-064>, 2010.

519 Keane, R. E., Reinhardt, E. D., Scott, J., Gray, K., and Reardon, J.: Estimating forest canopy bulk density using six  
520 indirect methods, *Can. J. For. Res.*, 35, 724–739, <https://doi.org/10.1139/x04-213>, 2005.

521 Keith, H., Mackey, B. G., and Lindenmayer, D. B.: Re-evaluation of forest biomass carbon stocks and lessons from  
522 the world’s most carbon-dense forests, *Proc. Natl. Acad. Sci.*, 106, 11635–11640,  
523 <https://doi.org/https://doi.org/10.1073/pnas.090197010>, 2009.

524 Lefsky, M. A., Cohen, W. B., Parker, G. G., and Harding, D. J.: Lidar remote sensing for ecosystem studies,  
525 *Bioscience*, 52, 19–30, [https://doi.org/10.1641/0006-3568\(2002\)052\[0019:LRSFES\]2.0.CO;2](https://doi.org/10.1641/0006-3568(2002)052[0019:LRSFES]2.0.CO;2), 2002.

526 Lefsky, M. A., Hudak, A. T., Cohen, W. B., and Acker, S. A.: Patterns of covariance between forest stand and  
527 canopy structure in the Pacific Northwest, *Remote Sens. Environ.*, 95, 517–531,  
528 <https://doi.org/10.1016/j.rse.2005.01.004>, 2005.

529 Li, Y., Andersen, H., and McGaughey, R.: A comparison of statistical methods for estimating forest biomass from  
530 light detection and ranging data, *West. J. Appl. For.*, 23, 223–231,  
531 <https://doi.org/https://doi.org/10.1093/wjaf/23.4.223>, 2008.

532 Magnussen, S. and Boudewyn, P.: Derivations of stand heights from airborne laser scanner data with canopy-based  
533 quantile estimators, *Can. J. For. Res.*, 28, 1016–1031, 1998.

534 Margolis, H. A., Nelson, R. F., Montesano, P. M., Beaudoin, A., Sun, G., Andersen, H. E., and Wulder, M. A.:  
535 Combining satellite lidar, airborne lidar, and ground plots to estimate the amount and distribution of aboveground  
536 biomass in the boreal forest of North America, *Can. J. For. Res.*, 45, 838–855, <https://doi.org/10.1139/cjfr-2015-0006>, 2015.

538 Martin-Ducup, O., Dupuy, J. L., Soma, M., Guerra-Hernandez, J., Marino, E., Fernandes, P. M., Just, A., Corbera,  
539 J., Touthkov, M., Sorribas, C., Bock, J., Piboule, A., Pirotti, F., and Pimont, F.: Unlocking the potential of Airborne  
540 LiDAR for direct assessment of fuel bulk density and load distributions for wildfire hazard mapping, *Agric. For.*  
541 *Meteorol.*, 362, <https://doi.org/10.1016/j.agrformet.2024.110341>, 2025.

542 Matasci, G., Hermosilla, T., Wulder, M. A., White, J. C., Coops, N. C., Hobart, G. W., and Zald, H. S. J.: Large-area  
543 mapping of Canadian boreal forest cover, height, biomass and other structural attributes using Landsat composites  
544 and lidar plots, *Remote Sens. Environ.*, 209, 90–106, <https://doi.org/10.1016/j.rse.2017.12.020>, 2018a.

545 Matasci, G., Hermosilla, T., Wulder, M. A., White, J. C., Coops, N. C., Hobart, G. W., Bolton, D. K., Tompalski, P.,  
546 and Bater, C. W.: Three decades of forest structural dynamics over Canada’s forested ecosystems using Landsat  
547 time-series and lidar plots, *Remote Sens. Environ.*, 216, 697–714, <https://doi.org/10.1016/j.rse.2018.07.024>, 2018b.

548 McGaughey, R. J.: FUSION/LDV: Software for LIDAR Data Analysis and Visualization,  
549 <http://forsys.sefs.uw.edu/fusion/fusionlatest.html>, 2024.

550 Moran, C. J., Kane, V. R., and Seielstad, C. A.: Mapping forest canopy fuels in the western United States with

551 LiDAR-Landsat covariance, *Remote Sens.*, 12, <https://doi.org/10.3390/rs12061000>, 2020.

552 Mutlu, M., Popescu, S. C., Stripling, C., and Spencer, T.: Mapping surface fuel models using lidar and multispectral  
553 data fusion for fire behavior, *Remote Sens. Environ.*, 112, 274–285, <https://doi.org/10.1016/j.rse.2007.05.005>, 2008.

554 Naesset, E.: Estimating above-ground biomass in young forests with airborne laser scanning, *Int. J. Remote Sens.*,  
555 32, 473–501, <https://doi.org/http://www.tandfonline.com/doi/abs/10.1080/01431160903474970>, 2011.

556 Næsset, E.: Predicting forest stand characteristics with airborne scanning laser using a practical two-stage procedure  
557 and field data, *Remote Sens. Environ.*, 80, 88–99, [https://doi.org/10.1016/S0034-4257\(01\)00290-5](https://doi.org/10.1016/S0034-4257(01)00290-5), 2002.

558 Næsset, E.: Practical large-scale forest stand inventory using a small-footprint airborne scanning laser, *Scand. J. For.*  
559 *Res.*, 19, 164–179, <https://doi.org/10.1080/02827580310019257>, 2004.

560 Natural Resources Canada: The State of Canada’s Forests: Annual Report 2023, Natural Resources Canada,  
561 Canadian Forest Service, Ottawa, Ontario., 116 pp., 2023.

562 Nelson, R.: How did we get here? An early history of forestry lidar, *Can. J. Remote Sens.*, 39, S6–S17,  
563 <https://doi.org/10.5589/m13-011>, 2013.

564 Nelson, R., Gobakken, T., Næsset, E., Gregoire, T. G., Ståhl, G., Holm, S., and Flewelling, J.: Lidar sampling -  
565 Using an airborne profiler to estimate forest biomass in Hedmark County, Norway, *Remote Sens. Environ.*, 123,  
566 563–578, <https://doi.org/10.1016/j.rse.2011.10.036>, 2012.

567 Nilsson, M.: Estimation of tree heights and stand volume using an airborne lidar system, *Remote Sens. Environ.*, 56,  
568 1–7, [https://doi.org/10.1016/0034-4257\(95\)00224-3](https://doi.org/10.1016/0034-4257(95)00224-3), 1996.

569 Ogle, S. M., Domke, G., Kurz, W. A., Rocha, M. T., Huffman, T., Swan, A., Smith, J. E., Woodall, C., and Krug,  
570 T.: Delineating managed land for reporting national greenhouse gas emissions and removals to the United Nations  
571 framework convention on climate change, *Carbon Balance Manag.*, 13,  
572 <https://doi.org/https://doi.org/10.1186/s13021-018-0095-3>, 2018.

573 Parisien, M. A., Barber, Q. E., Hirsch, K. G., Stockdale, C. A., Erni, S., Wang, X., Arseneault, D., and Parks, S. A.:  
574 Fire deficit increases wildfire risk for many communities in the Canadian boreal forest, *Nat. Commun.*, 11,  
575 <https://doi.org/10.1038/s41467-020-15961-y>, 2020.

576 Parisien, M. A., Barber, Q. E., Flannigan, M. D., and Jain, P.: Broadleaf tree phenology and springtime wildfire  
577 occurrence in boreal Canada, *Glob. Chang. Biol.*, 29, 6106–6119, <https://doi.org/10.1111/gcb.16820>, 2023.

578 Reutebuch, S. E., Anderson, H. E., and McGaughey, R. J.: Light detection and ranging (LIDAR): an emerging tool  
579 for multiple resource inventory, *J. For.*, 103, 286–292, 2005.

580 Riaño, D., Meier, E., Allgöwer, B., Chuvieco, E., and Ustin, S. L.: Modeling airborne laser scanning data for the  
581 spatial generation of critical forest parameters in fire behavior modeling, *Remote Sens. Environ.*, 86, 177–186,

582 [https://doi.org/10.1016/S0034-4257\(03\)00098-1](https://doi.org/10.1016/S0034-4257(03)00098-1), 2003.

583 Riaño, D., Chuvieco, E., Condés, S., González-Matesanz, J., and Ustin, S. L.: Generation of crown bulk density for  
584 *Pinus sylvestris* L. from lidar, *Remote Sens. Environ.*, 92, 345–352, <https://doi.org/10.1016/j.rse.2003.12.014>, 2004.

585 Roussel, J. R. and Auty, D.: *lidR: Airborne LiDAR Data Manipulation and Visualization for Forestry Applications*,  
586 <https://cran.r-project.org/package=lidR>, 2023.

587 Roussel, J. R., Auty, D., Coops, N. C., Tompalski, P., Goodbody, T. R. H., Meador, A. S., Bourdon, J. F., de  
588 Boissieu, F., and Achim, A.: *lidR: An R package for analysis of Airborne Laser Scanning (ALS) data*, *Remote Sens.*  
589 *Environ.*, 251, 112061, <https://doi.org/10.1016/j.rse.2020.112061>, 2020.

590 Shannon, C. E.: A mathematical theory of communication, *Bell Syst. Tech. J.*, 27, 379–423,  
591 <https://doi.org/10.1002/j.1538-7305.1948.tb01338.x>, 1948.

592 Shi, Y., Wang, J., and Kissling, W. D.: Multi-temporal high-resolution data products of ecosystem structure derived  
593 from country-wide airborne laser scanning surveys of the Netherlands, *Earth Syst. Sci. Data*, 17, 3641–3677,  
594 <https://doi.org/10.5194/essd-17-3641-2025>, 2025.

595 Singh, K. K., Chen, G., Vogler, J. B., and Meentemeyer, R. K.: When big data are too much: effects of LiDAR  
596 returns and point density on estimation of forest biomass, *IEEE J. Sel. Top. Appl. Earth Obs. Remote Sens.*, 9,  
597 3210–3218, <https://doi.org/10.1109/JSTARS.2016.2522960>, 2016.

598 Solberg, S., Næsset, E., Hanssen, K. H., and Christiansen, E.: Mapping defoliation during a severe insect attack on  
599 Scots pine using airborne laser scanning, *Remote Sens. Environ.*, 102, 364–376,  
600 <https://doi.org/10.1016/j.rse.2006.03.001>, 2006.

601 Stefanidou, A., Gitas, I. Z., Korhonen, L., Stavrakoudis, D., and Georgopoulos, N.: LiDAR-based estimates of  
602 canopy base height for a dense uneven-aged structured forest, *Remote Sens.*, 12, 1–20,  
603 <https://doi.org/10.3390/rs12101565>, 2020.

604 Stinson, G., Thandi, G., Aitkin, D., Bailey, C., Boyd, J., Colley, M., Fraser, C., Gelhorn, L., Groenewegen, K.,  
605 Hogg, A., Kapron, J., Leboeuf, A., Makar, M., Montigny, M., Pittman, B., Price, K., Salkeld, T., Smith, L.,  
606 Viveiros, A., and Wilson, D.: A new approach for mapping forest management areas in Canada, *For. Chron.*, 95,  
607 101–112, <https://doi.org/10.5558/tfc2019-017>, 2019.

608 Tews, J., Brose, U., Grimm, V., Tielbörger, K., Wichmann, M. C., Schwager, M., and Jeltsch, F.: Animal species  
609 diversity driven by habitat heterogeneity/diversity: The importance of keystone structures, *J. Biogeogr.*, 31, 79–92,  
610 <https://doi.org/10.1046/j.0305-0270.2003.00994.x>, 2004.

611 Tompalski, P.: *lidRmetrics*, <https://github.com/ptompalski/lidRmetrics>, 2024.

612 Tompalski, P., Hermosilla, T., Baral, S. K., Wulder, M. A., and White, J. C.: National remote sensing-derived

613 aboveground biomass yield curves for Canada, *For. An Int. J. For. Res.*, cpaf067,  
614 <https://doi.org/10.1093/forestry/cpaf067>, 2025.

615 Vogelmann, J. E., Howard, S. M., Yang, L., Larson, C. R., Wylie, B. K., and VanDriel, N.: Completion of the 1990s  
616 National Land Cover Data set for the conterminous United States from Landsat Thematic Mapper data and ancillary  
617 data sources, *Photogramm. Eng. Remote Sensing*, June, 650–662, 2001.

618 Wells, J. V., Dawson, N., Culver, N., Reid, F. A., and Morgan Siegers, S.: The state of conservation in North  
619 America's Boreal Forest: issues and opportunities, *Front. For. Glob. Chang.*, 3, 1–18,  
620 <https://doi.org/10.3389/ffgc.2020.00090>, 2020.

621 White, J. C., Wulder, M. A., Varhola, A., Vastaranta, M., Coops, N. C., Cook, B. D., Pitt, D., and Woods, M.: A  
622 best practices guide for generating forest inventory attributes from airborne laser scanning data using an area-based  
623 approach, Natural Resources Canada, Canadian Forest Service, Canadian Wood Fibre Centre, Information Report  
624 FI-X-010, 50p. pp., 2013.

625 White, J. C., Wulder, M. A., Hobart, G. W., Luther, J. E., Hermosilla, T., Griffiths, P., Coops, N. C., Hall, R. J.,  
626 Hostert, P., Dyk, A., and Guindon, L.: Pixel-based image compositing for large-area dense time series applications  
627 and science, *Can. J. Remote Sens.*, 40, 192–212, <https://doi.org/10.1080/07038992.2014.945827>, 2014.

628 White, J. C., Tompalski, P., Vastaranta, M., Wulder, M. A., Saarinen, Stepper, C., and Coops, N. C.: A model  
629 development and application guide for generating an enhanced forest inventory using airborne laser scanning data  
630 and an area-based approach, [https://doi.org/DOI: 10.5558/tfc2013-132](https://doi.org/DOI:10.5558/tfc2013-132), 2017a.

631 White, J. C., Wulder, M. A., Hermosilla, T., Coops, N. C., and Hobart, G. W.: A nationwide annual characterization  
632 of 25 years of forest disturbance and recovery for Canada using Landsat time series, *Remote Sens. Environ.*, 194,  
633 303–321, <https://doi.org/10.1016/j.rse.2017.03.035>, 2017b.

634 White, J. C., Tompalski, P., Bater, C. W., Wulder, M. A., Fortin, M., Hennigar, C., Robere-McGugan, G., Sinclair,  
635 I., and White, R.: Enhanced forest inventories in Canada: implementation, status, and research needs, *Can. J. For.*  
636 *Res.*, 55, 1–37, <https://doi.org/10.1139/cjfr-2024-0255>, 2025.

637 Woods, M., Lim, K., and Treitz, P.: Predicting forest stand variables from LiDAR data in the Great Lakes - St.  
638 Lawrence forest of Ontario, *For. Chron.*, 84, 827–839, 2008.

639 Wulder, M. A., Bater, C. W., Coops, N. C., Hilker, T., and White, J. C.: The role of LiDAR in sustainable forest  
640 management, *For. Chron.*, 84, 807–826, <https://doi.org/10.5558/tfc84807-6>, 2008.

641 Wulder, M. A., White, J. C., Bater, C. W., Coops, N. C., Hopkinson, C., and Chen, G.: Lidar plots — a new large-  
642 area data collection option: context, concepts, and case study, *Can. J. Remote Sens.*, 38, 600–618,  
643 <https://doi.org/10.5589/m12-049>, 2012a.

644 Wulder, M. A., White, J. C., Nelson, R. F., Næsset, E., Ørka, H. O., Coops, N. C., Hilker, T., Bater, C. W., and

645 Gobakken, T.: Lidar sampling for large-area forest characterization: A review, *Remote Sens. Environ.*, 121, 196–  
646 209, <https://doi.org/10.1016/j.rse.2012.02.001>, 2012b.

647 Wulder, M. A., Hermosilla, T., White, J. C., Bater, C. W., Hobart, G., and Bronson, S. C.: Development and  
648 implementation of a stand-level satellite-based forest inventory for Canada, *For. An Int. J. For. Res.*, 97, 546–563,  
649 <https://doi.org/10.1093/forestry/cpad065>, 2024.

650 Zald, H. S. J., Wulder, M. A., White, J. C., Hilker, T., Hermosilla, T., Hobart, G. W., and Coops, N. C.: Integrating  
651 Landsat pixel composites and change metrics with lidar plots to predictively map forest structure and aboveground  
652 biomass in Saskatchewan, Canada, *Remote Sens. Environ.*, 176, 188–201, <https://doi.org/10.1016/j.rse.2016.01.015>,  
653 2016.

654